nature cell biology

# The mitotic kinesin-14 Ncd drives directional microtubule–microtubule sliding

Gero Fink[1,5], Lukasz Hajdo[2,3,5], Krzysztof J. Skowronek[2,4], Cordula Reuther[1], Andrzej A. Kasprzak[2] and Stefan Diez[1,6]

**During mitosis and meiosis, the bipolar spindle facilitates chromosome segregation through microtubule sliding as well as microtubule growth and shrinkage[1]. Kinesin-14, one of the motors involved, causes spindle collapse in the absence of kinesin-5 (refs 2, 3), participates in spindle assembly[4] and modulates spindle length[5]. However, the molecular mechanisms underlying these activities are not known. Here, we report that *Drosophila melanogaster* kinesin-14 (Ncd) alone causes sliding of anti-parallel microtubules but locks together (that is, statically crosslinks) those that are parallel. Using single molecule imaging we show that Ncd diffuses along microtubules in a tail-dependent manner and switches its orientation between sliding microtubules. Our results show that kinesin-14 causes sliding and expansion of an anti-parallel microtubule array by dynamic interactions through the motor domain on the one side and the tail domain on the other. This mechanism accounts for the roles of kinesin-14 in spindle organization.**

The mitotic spindle is a molecular machine composed of a bipolar array of microtubules whose minus ends are focused at the spindle poles and whose plus ends demarcate a midzone of overlapping microtubules with opposite polarity. This complex organization is achieved by the activity of molecular motors that generate forces directed towards the minus and plus ends of microtubules[6,7]. In particular, minus-end-directed motor proteins of the kinesin-14 family, which consist of a carboxy-terminal ATP-hydrolysing motor domain and an amino-terminal ATP-independent microtubule binding site[8–11], have been shown to have essential roles in spindle organization during meiosis[12–14] and mitosis[15–17]. Kinesin-14, whose function is highly conserved, specifically enriches at the spindle poles, but also localizes to spindle microtubules[4,17,18]. Malfunctioning of kinesin-14 during mitosis results in splayed multipolar spindles and unfocused spindle poles[4,18,19]. These defects are assumed to result from the microtubule crosslinking activity of kinesin-14, by which the motors form stable contacts between parallel-oriented microtubules near the spindle poles but cause sliding between anti-parallel microtubules in the midzone[4,17,19].

When kinesin-14 is depleted, slightly longer spindles[20] are observed at metaphase–anaphase A transition[21], suggesting an involvement of kinesin-14 in the modulation of spindle length. Conversely, cells lacking kinesin-5, a plus-end-directed microtubule motor capable of sliding microtubules relative to each other[22], have collapsed spindles[2,17,23]. In these studies, simultaneous inhibition of kinesin-14 restored centrosome separation and the formation of bipolar spindles. This antagonistic behaviour suggests that kinesin-14 counteracts kinesin-5 by an oppositely directed microtubule–microtubule sliding mechanism. Consistent with this prediction, recent experiments in which Ncd was overexpressed showed an increase in motility of microtubule bundles[24].

To elucidate the interaction of Ncd motors with microtubules on the single molecule level, we developed an *in vitro* assay that reduces non-specific adhesion of motor proteins to the substrate surface (Fig. 1). Given that Ncd translocates on microtubules in a non-processive manner[25,26], we expected that the motors would interact predominantly with the 'template' microtubules through their N-terminal microtubule binding sites (Fig. 1a). Using total internal reflection fluorescence (TIRF) microscopy we observed that GFP-labelled Ncd (full-length GFP–Ncd) indeed colocalized with the template microtubules (Fig. 1b, c). To investigate whether tail-mediated interaction of Ncd with microtubules involved static binding (as suggested by a recent *in vitro* study[27]) or was dynamic, we performed single-molecule experiments (Fig. 1d). Surprisingly, a high proportion of the full-length motor (identified as dimeric molecules; Supplementary Information, Figs S1, S2) diffused along the microtubule. To test which parts of the protein were required for the diffusional motion, we constructed truncated, dimeric Ncd motors, which lacked either the second microtubule binding site (tailless, GFP–Ncd$^{195}$) or the motor domain (headless Ncd$^{349}$–GFP). We observed only very short events of transient binding for the tailless GFP–Ncd$^{195}$. Diffusion of this protein construct was never observed, indicating that neither the head nor the stalk or GFP alone mediate diffusion. Interestingly, we did not observe any stationary binding of headless Ncd$^{349}$–GFP. Instead, this construct diffused robustly along the microtubule. When repeating these experiments in the presence of AMP–PNP (adenyl-5′-yl imidodiphosphate; Supplementary

[1]Max Planck Institute of Molecular Cell Biology and Genetics, Pfotenhauerstraβe 108, 01307 Dresden, Germany. [2]Nencki Institute of Experimental Biology, 3 Pasteur St., 02-093 Warsaw, Poland. [3]Department of General Biophysics, University of Lodz, 12/16 Banacha St., 90-237 Lodz,Poland. [4]International Institute of Molecular and Cell Biology, 4 Trojdena St., 02-093 Warsaw, Poland.
[5]These authors contributed equally to this work.
[6]Correspondence should be addressed to S.D. (e-mail: diez@mpi-cbg.de)

Received 3 December 2008; accepted 23 February 2009; published online 10 May 2009; DOI: 10.1038/ncb1877

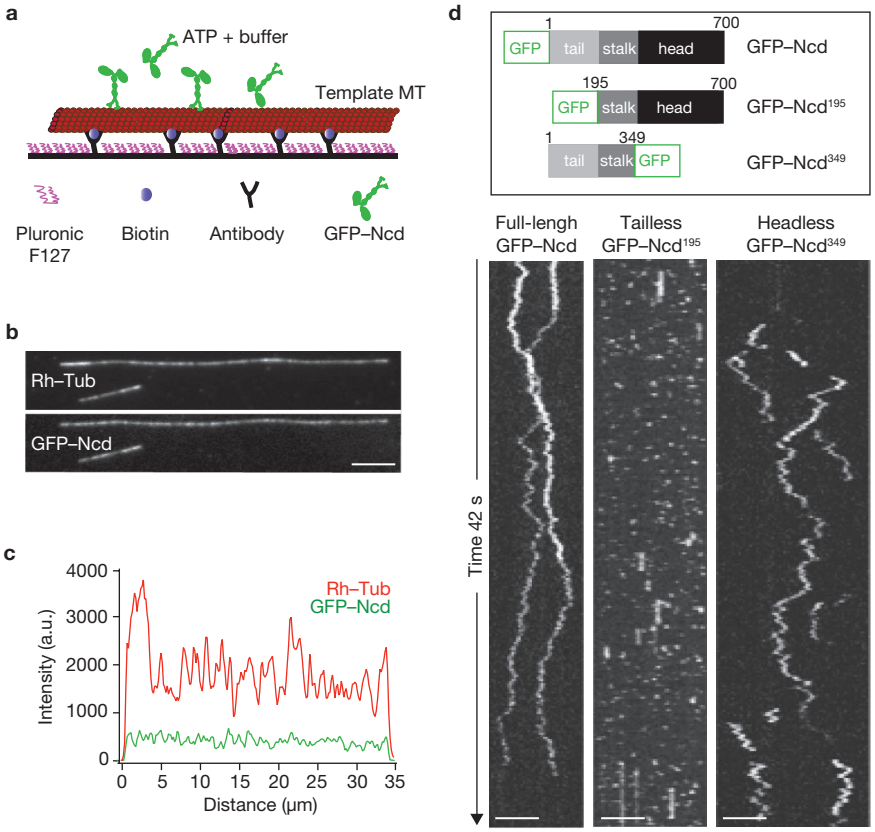


**Figure 1** Ncd interaction with microtubules in the presence of ATP. (**a**) Diagram of the experimental setup. 'Template' microtubules (MT; dimly rhodamine-labelled) were tagged with biotin and immobilized to the glass surface by α-biotin antibodies. To block non-specific surface binding of Ncd motors, the surface was coated with Pluronic F127. These template microtubules were then incubated with Ncd motors. (**b**) Epifluorescence and TIRF microscopy images of rhodamine-labelled template microtubules (Rh–Tub) and interacting GFP-labelled full-length Ncd motors (GFP–Ncd). Scale bar, 5 μm. (**c**) Line scan analysis showing the fluorescence intensity profiles of the long template microtubule in B (red) with the corresponding GFP–Ncd signal (green). (**d**) Kymographs of different, single-molecule GFP-labelled Ncd constructs imaged by TIRF microscopy in the presence of 1 mM ATP. Full-length GFP–Ncd diffused along the microtubule. Tailless GFP–Ncd$^{195}$ revealed short-lived binding events (characteristic for head–microtubule interactions of a non-processive motor) but never diffused along the microtubule lattice. Occasional events of short-term stationary binding were probably related to degraded motors with impaired ATP hydrolysis. Headless Ncd$^{349}$–GFP also diffused along the microtubules. We note, that any potential interaction between the Ncd tail and the GFP in the N-terminal region of the protein can be ruled out as the origin for the diffusive interaction because the GFP is attached on the C-terminal side in Ncd$^{349}$–GFP. Our high ionic strength experiments complement earlier studies[27]. There, the tail domains of Ncd were suggested to be responsible for static binding, as well as directed motility, of full-length Ncd at low ionic strength. However, no headless constructs were tested and no experiments with full-length Ncd at high ionic strength were conducted in their study. Scale bars, 3 μm. (Supplementary Information, Movies 1–3)

Information, Fig. S3), the diffusion of the headless Ncd$^{349}$–GFP was not affected. In contrast, full-length Ncd and tailless GFP–Ncd$^{195}$ both showed extended periods of stationary binding. From these observations, we conclude that tailless GFP–Ncd$^{195}$ interacts predominantly with the microtubule through its motor heads in an ATP-dependent manner, and that the Ncd tail alone is capable of mediating diffusion along the microtubule. This tail-dependent diffusion makes the protein a highly dynamic microtubule crosslinker and raises the question of whether Ncd can indeed induce microtubule–microtubule sliding.

To investigate Ncd-induced microtubule–microtubule interactions we again used the assay described in Fig. 1. Individual 'transport' microtubules then landed on the Ncd-covered template microtubules (Fig. 2a). Of the microtubule–microtubule interaction events ($n = 209$), 52.2% of the transport microtubules showed robust sliding (Fig. 2b, c, arrowheads), 37.8% showed only short motility and slowed down exponentially before stopping (Supplementary Information, Fig. S4) and 10% statically crosslinked to the template microtubules immediately after landing (Fig. 2c, arrow). Robust sliding always occurred in the opposite direction along the template microtubules, compared with the short motility events. Additional support for this phenomenon was provided by a number of transport microtubules sliding robustly to the end of the template microtubule, where they performed nodal-end swivelling and crosslinked statically after reorientation (Fig. 2c, asterisk). This suggests a directional sliding mechanism, where oppositely oriented transport microtubules behave differently in their interaction with an individual template microtubule. By contrast, tailless GFP–Ncd$^{195}$ and headless Ncd$^{349}$–GFP did not induce any specific microtubule–microtubule interactions, indicating that both, Ncd motor and tail domains are compulsory for microtubule–microtubule sliding and crosslinking.

To determine the polarity of the interacting microtubules, we first determined the orientation of the transport microtubules by polarity-marking (Fig. 2a–c; Supplementary Information, Fig. S5). Next we determined the orientation of the template microtubules by imaging

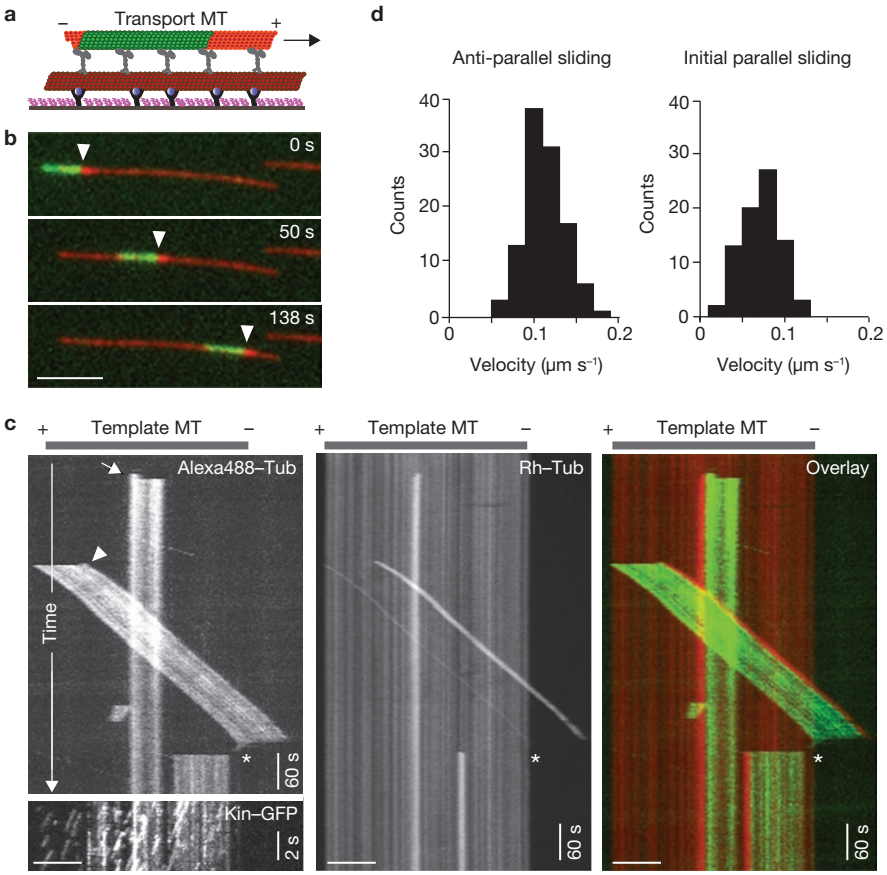


**Figure 2** Ncd induces directional microtubule–microtubule sliding and static crosslinking. (**a**) Diagram of a polarity-marked 'transport' microtubule (MT) interacting with a Ncd-decorated template microtubule. After incubation of the dimly-labelled template microtubules with full-length Ncd (GFP–Ncd or unlabelled Ncd), we extensively washed the flowcell to remove free Ncd motor from solution and added non-biotinylated, either polarity-marked or non-marked (brightly-labelled with rhodamine) transport microtubules in ATP-containing motility buffer. Polarity-marked microtubules were composed of Alexa488–tubulin seeds (Alexa488–Tub; green) and rhodamine–tubulin extensions (Rh–Tub; red), with the longer extension marking the plus end of the microtubule. (**b**) Time-lapse fluorescence micrographs of a polarity-marked transport microtubule (arrowheads) robustly sliding along a rhodamine-labelled (dim red) template microtubule. (**c**) Multi-channel kymographs illustrating the dynamic interactions of polarity-marked transport microtubules with a template microtubule (schematically depicted above the kymographs). The polarity of the template microtubule was determined by GFP-labelled kinesin-1 molecules, moving towards the microtubule plus ends (lower left panel, horizontal scale bar for all kymographs, 5 μm). Robust sliding of transport microtubules occurred exclusively with their plus ends leading towards the minus ends of the template microtubules (arrowhead). After reaching the microtubule end, the transport microtubule shown swivelled for a short time, reoriented and was stuck (asterisk). Transport microtubules that were oriented in the opposite direction showed only short motility or statically crosslinked immediately after landing (arrow). (Supplementary Information, Movie 4). (**d**) Histograms of sliding velocities for anti-parallel (0.11 ± 0.02 μm $s^{-1}$, mean ± s.d., $n = 109$) and parallel (0.07 ± 0.02 μm $s^{-1}$, mean ± s.d., $n = 79$) microtubule arrangements. For the parallel microtubule arrangement, sliding velocities were averaged during the first 10 s after landing of the transport microtubule.

the plus-end-directed motion of single GFP-labelled kinesin-1 molecules (Fig. 2c; Supplementary Information, Fig. S5) after the Ncd-mediated microtubule–microtubule sliding experiments. From these experiments, we conclude that the events of robust sliding always corresponded to an anti-parallel arrangement of template and transport microtubules, whereas parallel microtubule arrangements led to only short (or no) motility. Quantitative analysis revealed a sliding velocity of 0.11 ± 0.02 μm $s^{-1}$ (mean ± s.d., $n = 109$ microtubules) for anti-parallel microtubules (Fig. 2d). Parallel sliding, during the first 10 s after landing of the transport microtubule, revealed a sliding velocity of 0.07 ± 0.02 μm $s^{-1}$ (mean ± s.d., $n = 79$ microtubules). However, after 100 s, 69% of the parallel transport microtubules (which did not reach a microtubule end, or interacted with other transport microtubules) had stopped. To determine whether single motor molecules continue diffusing during microtubule–microtubule sliding, we performed spiking experiments, where GFP–Ncd was mixed with unlabelled (full-length) Ncd. We never observed any obvious conversion from diffusion to directional motion or from diffusion to static binding (Supplementary Information, Fig. S6).

To understand the role of Ncd in the difference between robust sliding of anti-parallel microtubules and the slowing down of parallel microtubules, we performed dual-colour TIRF microscopy and imaged GFP–Ncd simultaneously with the fluorescent signals of the interacting microtubules (Fig. 3). As expected, the template microtubules were well-decorated with GFP–Ncd; however, we were surprised to find that the transport microtubules also carried a pronounced GFP–Ncd signal during anti-parallel sliding (Fig. 3a, b). In our experiments we aimed at removing free GFP–Ncd in the flowcell before perfusion of the transport microtubules; this raises the question of how motors accumulate on the transport microtubule. We therefore analysed the landing of transport microtubules on template microtubules and found that in 52.6% ($n = 38$

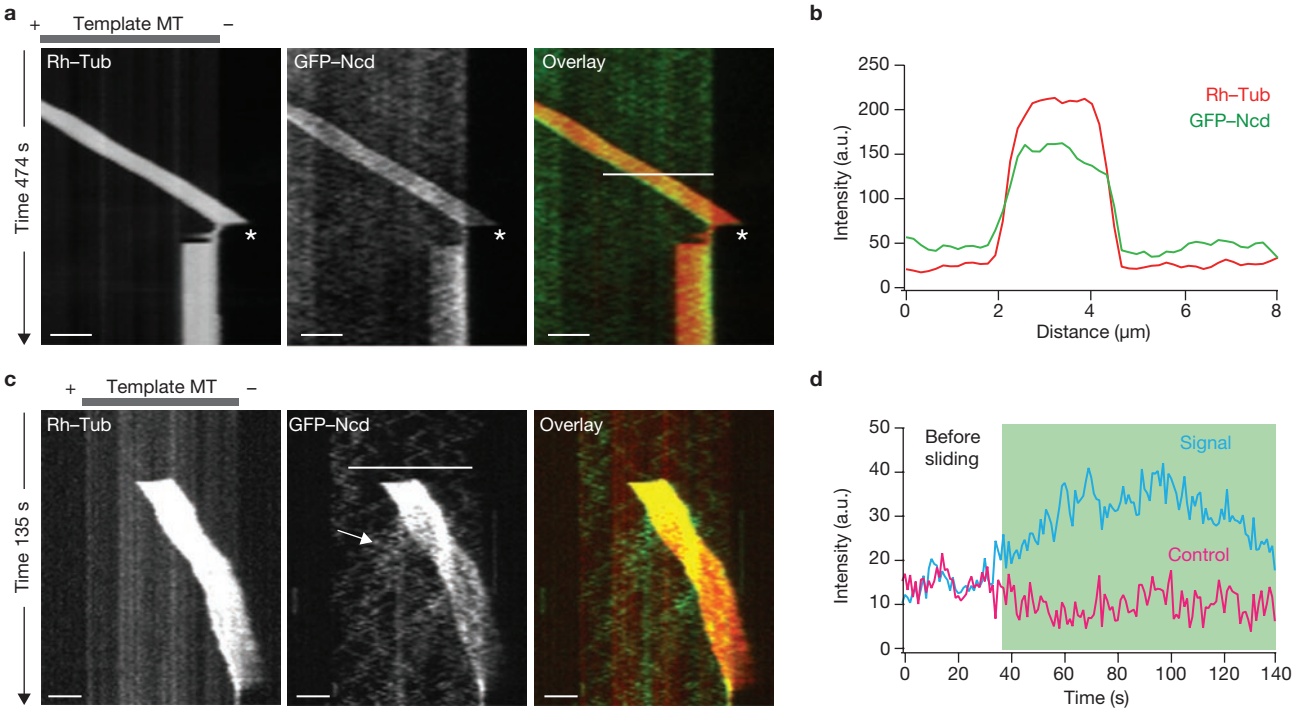


**Figure 3** Transport and switching of Ncd during sliding. (**a**) Dual-colour kymographs of an anti-parallel sliding event where transport microtubules (MT) without Ncd were subjected to Ncd-decorated template microtubules. The transport microtubule reorients and statically crosslinks after nodal end swivelling (asterisk). GFP–Ncd is clearly associated with the transport microtubule during sliding and static crosslinking. Scale bars, 3 μm. (**b**) Fluorescence intensity profiles of the sliding transport microtubule (red) with the corresponding GFP–Ncd signal (green). GFP–Ncd is evenly distributed over the whole length of the microtubule. The regions from which the intensity values were taken are indicated by a white line in **a**. (**c**) Dual-colour kymographs of a sliding event where transport microtubules (decorated with GFP–Ncd) were subjected to template microtubules that had not been decorated with GFP–Ncd before. In this way, we reduced the otherwise high GFP–Ncd background along the template microtubules. During sliding, GFP–Ncd switches from the transport microtubule to the template microtubule (arrow). The faint GFP signal already present on the template microtubule before the sliding event is attributed to the earlier landing of residual GFP–Ncd out of solution. In some cases, anti-parallel sliding did not occur as a continuous smooth movement and periods of slightly changing velocities were observed. The origin of these effects remain speculative: in principle a transient slow-down in the movement could arise from the involvement of an increased number of dead (or less active) motors, or from motor hindering (crowding) effects under conditions of high Ncd concentrations. Scale bars, 3 μm. (Supplementary Information, Movie 5). (**d**) Averaged GFP–Ncd fluorescence intensities as a function of time along a template microtubule where a GFP–Ncd-decorated transport microtubule had landed (blue, averaged signal along the white line in **c** and along the two nearest control microtubules without landing events (red). The strong GFP–Ncd signal associated with the transport microtubule during sliding was not considered in the averaging process. The signal increase during microtubule–microtubule sliding (blue curve in the shaded time interval) indicates the transfer of GFP–Ncd from the transport microtubule to the template microtubule.

anti-parallel transport microtubules) of the events, the transport microtubules carried no motors. However, the motor signal along the transport microtubule then rapidly increased, suggesting that Ncd is picked up from the template microtubule during sliding. We confirmed the pickup of motors by the transport microtubule from the template microtubule by single molecule experiments (Supplementary Information, Fig. S7). In 47.4% of the landing events, transport microtubules were already weakly decorated with motors. This decoration presumably originated from residual motors in solution or from the pickup of motors from other template microtubules during previous sliding events.

To further investigate the transfer of motors between sliding microtubules, we mixed transport microtubules with GFP–Ncd in ATP-containing motility solution and added them to non-decorated template microtubules. Analysis of the GFP–Ncd signal after the landing of individual transport microtubules revealed that GFP–Ncd was left behind on the template microtubule during anti-parallel sliding (Fig. 3c, d). The fact that the transferred GFP–Ncd did not remain localized in the areas passed by the transport microtubule can be explained by the diffusive interaction of GFP–Ncd with the template microtubule. We confirmed the described transfer behaviour by single-molecule experiments. We found, moreover, that transfer did not depend on the relative orientation of the microtubules to each other. However, transfer ceased when Ncd interacted more permanently with the microtubules through their motor domains in the presence of AMP–PNP (Supplementary Information, Fig. S7).

Although we did not observe any motor accumulations at either end of the transport microtubule during anti-parallel sliding, GFP–Ncd accumulated at the minus ends of parallel microtubules after reorientation and static parallel crosslinking (Fig. 3a), as well as during the slow-down after landing (Fig. 4a). In the latter, end-accumulation was not observed immediately but rather, developed over time (Fig. 4b). Overall, such accumulations were detected in 28 of 29 parallel, statically crosslinked microtubule bundles. Moreover, the end accumulation shifted to the new minus end of the microtubule-bundle when a second microtubule overlapped with an existing microtubule bundle in a parallel manner (Fig. 4c). Because this end accumulation was never observed on single or anti-parallel microtubules, we conclude that Ncd accumulations are specific for parallel microtubule bundles.

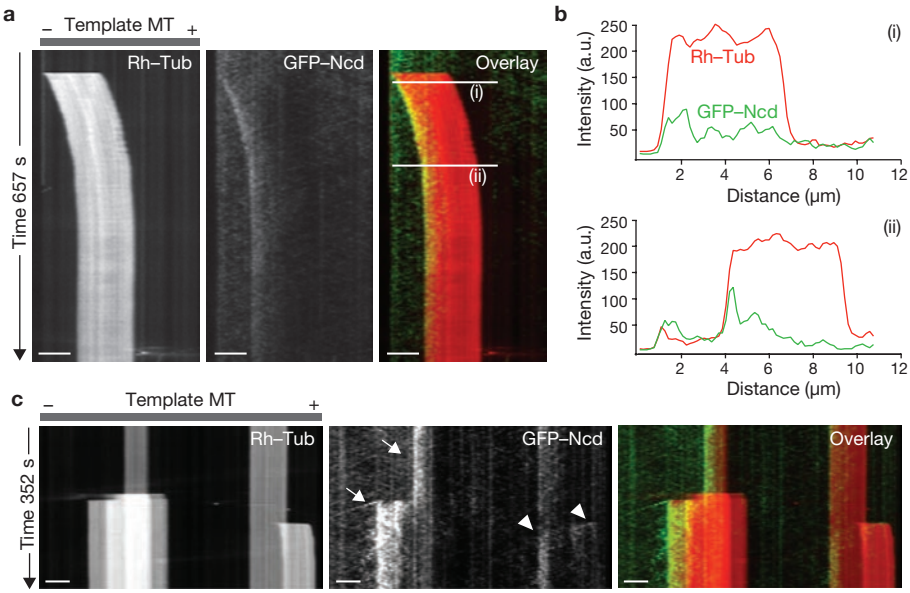


**Figure 4** Accumulation of Ncd at the minus ends of parallel microtubule-bundles. (**a**) Dual-colour kymographs of a parallel sliding event where transport microtubules (MT) without Ncd were subjected to GFP–Ncd-decorated template microtubules. Shortly after landing, the GFP–Ncd signal was evenly distributed over the length of the transport microtubule (i), and during and after slow-down a pronounced minus end accumulation was observed (ii). Scale bars, 3 μm. (Supplementary Information, Movie 6). (**b**) Fluorescence intensity profiles (along the white lines in **a**) of the transport microtubule (red) and the corresponding GFP–Ncd signal (green). (**c**) Dual-colour kymographs of microtubule landing events on statically crosslinked, parallel microtubules. Additional GFP–Ncd was shuttled to the minus end of a parallel microtubule-bundle upon the binding of another (spatially overlapping) parallel microtubule (arrowheads). An already existing GFP–Ncd minus end accumulation shifts to the new, peripheral minus-end of the total bundle (arrows). The faint line of GFP–Ncd signal appearing as processive movement towards the minus end of the template microtubule was presumably related to the formation of occasional GFP–Ncd clusters emerging from the motor accumulations at minus ends of the parallel microtubule-bundles.

In our experiments, we directly showed that Ncd alone facilitates robust anti-parallel microtubule–microtubule sliding, whereas it statically crosslinks parallel microtubules. In the case of anti-parallel microtubules, the motors linked through their tail domains to the transport microtubule ('transport motors') push the transport microtubule in the same direction as the motors bound to the template microtubule ('template motors'). Conversely, static crosslinking of parallel microtubules is caused by a tug-of-war where motors work against each other (Fig. 5). Thus, our results suggest that Ncd can mediate spindle collapse in the absence of kinesin-5 by a microtubule–microtubule sliding mechanism. In addition, the motor characteristics described explain how kinesin-14 and kinesin-5 modulate spindle length at a metaphase–anaphase transition[21] and that motor activity is needed to organize microtubules into a parallel array near the spindle poles[28].

The directional sliding mechanism described here is accomplished by the cumulative recruitment of motors from one microtubule to the other. We showed that switching of motors between microtubules is facilitated by their rather loose, diffusive tail–microtubule interactions. *In vivo*, the dynamic switching of motors between microtubules might help to equilibrate the motor number on interacting kinetochore and spindle microtubules with initially asymmetric motor distributions. Such a mechanism would ensure that only parallel microtubules are statically crosslinked. In line with our work Braun and colleagues demonstrated *in vitro* that the kinesin-14 klp2 has the capability to organize microtubules into a parallel array (published in this issue; *Nature Cell Biol.* **11,** 724–730; 2009).

Our observation that Ncd molecules diffused in the microtubule overlap region during sliding shows that a diffusing motor can exert sliding forces. This is probably because the duration of the powerstroke is much shorter than tail-mediated diffusion. Moreover, diffusion of individual motors might be cancelled if multiple motors are simultaneously involved in transport. Using the same argument of collective but uncoordinated diffusion, static crosslinking between parallel microtubules can be explained. However, because it is difficult to determine which of the imaged motors are in fact actively involved in the microtubule–microtubule sliding process, we cannot rule out the possibility that the state of interaction differs for Ncd molecules involved in sliding from those that are not. It could be possible that Ncd is activated by microtubule crosslinking, similarly to kinesin-5 (ref. 29), leading to a different interaction mode during sliding.

Although the effect of Ncd in driving microtubule sliding seems similar to that seen with kinesin-5, the sliding mechanism is different. Kinesin-5 motors move processively on both microtubules at the same time and crosslink microtubules preferentially in an anti-parallel manner[22,30]. Accordingly, in *Drosophila* embryos and *Xenopus leavis* egg extract spindles, kinesin-5 molecules were observed to bind in a stationary manner between interpolar spindle microtubules during spindle elongation[31,32]. By contrast, Ncd diffuses along microtubules with its tail domain, but generates directed force with its head domain. Stationary localization of Ncd molecules in the spindle midzone is therefore not expected. Rather, Ncd is thought to be co-translocated with the sliding microtubules.

Consistent with previous studies[25,26], our single-molecule experiments did not indicate processivity of Ncd. However, Ncd accumulated at the minus ends between statically crosslinked parallel microtubules, consistent with the localization and function of Ncd at spindle poles and

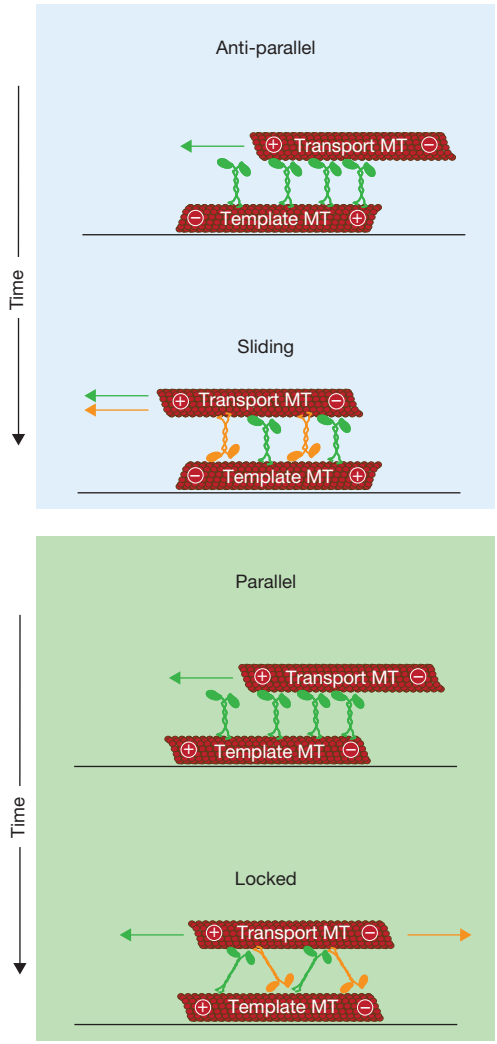


**Figure 5** Model for directional sliding and static crosslinking of microtubules by Ncd. For both, parallel and anti-parallel microtubules (MT), motors linked to the template microtubule (green motors) through their tail domains will be able to propel transport microtubules with their plus ends leading. Due to the loose binding of the motors, part of the Ncd molecules will switch with their tail to the transport microtubules (orange motors). Coloured arrows represent the forces on the transport microtubules generated by the respective motors. For anti-parallel sliding, motors pull (orange motors) and push (green motors) the transport microtubule in the same direction. Thus their action is assisting and facilitates sliding. For parallel sliding, motors pull (orange motors) and push (green motors) the transport microtubule in opposite directions. Thus the motors engage in a tug-of-war. Over time, switching of motors from template to transport microtubules leads to an increasing number of counteracting motors and causes slow-down of initially sliding parallel microtubules. Events of immediate static crosslinking after landing were presumably related to transport microtubules that had already picked up a sufficiently high number of Ncd molecules from solution or during previous sliding events.

centrosomes[18]. But how does Ncd reach the microtubule minus end and stay there? Obviously, the existence of a parallel microtubule bundle is a prerequisite for end-accumulation. Recently it has been suggested (using truncated constructs) that Ncd could become weakly processive when simultaneously interacting with multiple microtubules[27]; however, we did not observe such behaviour. Rather, we favour the idea that full-length Ncd could undergo a kind of biased diffusion between parallel microtubules. Moreover, internal strain built up in the Ncd molecules during the tug-of-war could influence crucial motor parameters, such as binding and unbinding rates of the motor head or tail domains.

In recent *in vivo* FRAP experiments, recovery of Ncd on kinetochore microtubules along with a prominent microtubule plus-end localization was reported[18]. We hypothesize that the dynamic interactions observed in our experiments might provide an explanation for the fast recovery. Moreover, Ncd might use one-dimensional diffusion to reach the microtubule plus end, which is similar to the end-targeting mechanism of kinesin-13 (ref. 33). In summary, we believe that the tail-dependent diffusion of motors, which are also able to exert directed force through their head domains, could be a general mechanism by which motors organize cellular structures. □

*Note added in proof: a related manuscript by Braun* et al. *(*Nature Cell Biol. ***11,*** *724–730; 2009) is also published in this issue.*

## METHODS

Methods and any associated references are available in the online version of the paper at http://www.nature.com/naturecellbiology/

*Note: Supplementary Information is available on the Nature Cell Biology website.*

### ACKNOWLEDGEMENTS

We acknowledge the members of the Kasprzak and the Diez labs for comments on the manuscript as well as C. Bräuer and D. Naumburger for technical support. We thank C. Leduc, B. Nitzsche, C. Gell and J. Howard for fruitful discussion, F. Ruhnow for help with the microtubule tracking, as well as S. Bajer and E. Kocik for help with FPLC experiments. This work was supported by the German Federal Ministry of Education and Research (Grant 03 N 8712), the Polish Network for Mechanisms of Cell Motility, the Grant 2 P04C 131 29 and the Max-Planck-Society. G. Fink was supported by a fellowship from the Boehringer Ingelheim Foundation

### AUTHOR CONTRIBUTIONS

G.F., L.H., C.R., A.A.K. and S.D. designed the experiments; L.H. and C.R. performed initial experiments; G.F. performed the presented experiments and analysed the data; L.H. and K.J.S. generated the Ncd proteins; G.F and S.D. wrote the manuscript; A.A.K. and S.D. initiated the research and supervised the work. All authors discussed the results and commented on the manuscript.

### COMPETING FINANCIAL INTERESTS

The authors declare no competing financial interests.

Published online at http://www.nature.com/naturecellbiology/
Reprints and permissions information is available online at http://npg.nature.com/reprintsandpermissions/

1. Gadde, S. & Heald, R. Mechanisms and molecules of the mitotic spindle. *Curr. Biol.* **14,** 797–805 (2004).
2. Sharp, D. J., Yu, K. R., Sisson, J. C., Sullivan, W. & Scholey, J. M. Antagonistic microtubule-sliding motors position mitotic centrosomes in *Drosophila* early embryos. *Nature Cell Biol.* **1,** 51–54 (1999).
3. Hoyt, M. A., He, L., Loo, K. K. & Saunders, W. S. Two *Saccharomyces cerevisiae* kinesin-related gene products required for mitotic spindle assembly. *J. Cell Biol.* **118,** 109–120 (1992).
4. Walczak, C. E., Verma, S. & Mitchison, T. J. XCTK2: a kinesin-related protein that promotes mitotic spindle assembly in *Xenopus laevis* egg extracts. *J. Cell Biol.* **136,** 859–870 (1997).
5. Sharp, D. J. *et al.* Functional coordination of three mitotic motors in *Drosophila* embryos. *Mol. Biol. Cell* **11,** 241–253 (2000).
6. Hildebrandt, E. R. & Hoyt, M. A. Mitotic motors in *Saccharomyces cerevisiae*. *Biochim. Biophys. Acta* **1496,** 99–116 (2000).
7. Sharp, D. J., Rogers, G. C. & Scholey, J. M. Microtubule motors in mitosis. *Nature* **407,** 41–47 (2000).
8. Chandra, R., Salmon, E. D., Erickson, H. P., Lockhart, A. & Endow, S. A. Structural and functional domains of the *Drosophila* ncd microtubule motor protein. *J. Biol. Chem.* **268,** 9005–9013 (1993).
9. McDonald, H. B. & Goldstein, L. S. Identification and characterization of a gene encoding a kinesin-like protein in *Drosophila*. *Cell* **61,** 991–1000 (1990).
10. McDonald, H. B., Stewart, R. J. & Goldstein, L. S. The kinesin-like ncd protein of *Drosophila* is a minus end-directed microtubule motor. *Cell* **63,** 1159–1165 (1990).

11. Karabay, A. & Walker, R. A. Identification of microtubule binding sites in the Ncd tail domain. *Biochemistry* **38,** 1838–1849 (1999).
12. Matthies, H. J., McDonald, H. B., Goldstein, L. S. & Theurkauf, W. E. Anastral meiotic spindle morphogenesis: role of the non-claret disjunctional kinesin-like protein. *J. Cell Biol.* **134,** 455–464 (1996).
13. Kimble, M. & Church, K. Meiosis and early cleavage in *Drosophila melanogaster* eggs: effects of the claret-non-disjunctional mutation. *J. Cell Sci.* **62,** 301–318 (1983).
14. Segbert, C. *et al.* KLP-18, a Klp2 kinesin, is required for assembly of acentrosomal meiotic spindles in *Caenorhabditis elegans*. *Mol. Biol. Cell* **14,** 4458–4469 (2003).
15. Hatsumi, M. & Endow, S. A. Mutants of the microtubule motor protein, nonclaret disjunctional, affect spindle structure and chromosome movement in meiosis and mitosis. *J. Cell Sci.* **101,** 547–559 (1992).
16. Saunders, W. S. & Hoyt, M. A. Kinesin-related proteins required for structural integrity of the mitotic spindle. *Cell* **70,** 451–458 (1992).
17. Mountain, V. *et al.* The kinesin-related protein, HSET, opposes the activity of Eg5 and cross-links microtubules in the mammalian mitotic spindle. *J. Cell Biol.* **147,** 351–366 (1999).
18. Goshima, G., Nedelec, F. & Vale, R. D. Mechanisms for focusing mitotic spindle poles by minus end-directed motor proteins.[see comment]. *J. Cell Biol.* **171,** 229–240 (2005).
19. Endow, S. A., Chandra, R., Komma, D. J., Yamamoto, A. H. & Salmon, E. D. Mutants of the *Drosophila* ncd microtubule motor protein cause centrosomal and spindle pole defects in mitosis. *J. Cell Sci.* **107,** 859–867 (1994).
20. Troxell, C. L. *et al.* pkl1$^{+}$and klp2$^{+}$: Two kinesins of the Kar3 subfamily in fission yeast perform different functions in both mitosis and meiosis. *Mol. Biol. Cell* **12,** 3476–3488 (2001).
21. Brust-Mascher, I. & Scholey, J. M. Microtubule flux and sliding in mitotic spindles of *Drosophila* embryos. *Mol. Biol. Cell* **13,** 3967–3975 (2002).
22. Kapitein, L. C. *et al.* The bipolar mitotic kinesin Eg5 moves on both microtubules that it crosslinks. *Nature* **435,** 114–118 (2005).
23. Hoyt, M. A., He, L., Totis, L. & Saunders, W. S. Loss of function of *Saccharomyces cerevisiae* kinesin-related CIN8 and KIP1 is suppressed by KAR3 motor domain mutations. *Genetics* **135,** 35–44 (1993).
24. Oladipo, A., Cowan, A. & Rodionov, V. Microtubule motor Ncd induces sliding of microtubules *in vivo*. *Mol. Biol. Cell* **18,** 3601–3606 (2007).
25. Foster, K. A. & Gilbert, S. P. Kinetic studies of dimeric Ncd: evidence that Ncd is not processive. *Biochemistry* **39,** 1784–1791 (2000).
26. Case, R. B., Pierce, D. W., Hom-Booher, N., Hart, C. L. & Vale, R. D. The directional preference of kinesin motors is specified by an element outside of the motor catalytic domain. *Cell* **90,** 959–966 (1997).
27. Furuta, K. & Toyoshima, Y. Y. Minus-end-directed motor Ncd exhibits processive movement that is enhanced by microtubule bundling *in vitro*. *Curr. Biol.* **18,** 152–157 (2008).
28. Walczak, C. E., Vernos, I., Mitchison, T. J., Karsenti, E. & Heald, R. A model for the proposed roles of different microtubule-based motor proteins in establishing spindle bipolarity. *Curr. Biol.* **8,** 903–913 (1998).
29. Kapitein, L. C. *et al.* Microtubule cross-linking triggers the directional motility of kinesin-5. *J. Cell Biol.***182,** 421–428 (2008).
30. van den Wildenberg, S. M. *et al.* The homotetrameric kinesin-5 KLP61F preferentially crosslinks microtubules into antiparallel orientations. *Curr. Biol.* **18,** 1860–1864 (2008).
31. Cheerambathur, D. K., Brust-Mascher, I., Civelekoglu-Scholey, G. & Scholey, J. M. Dynamic partitioning of mitotic kinesin-5 cross-linkers between microtubule-bound and freely diffusing states. *J. Cell Biol.* **182,** 429–436 (2008).
32. Uteng, M., Hentrich, C., Miura, K., Bieling, P. & Surrey, T. Poleward transport of Eg5 by dynein-dynactin in *Xenopus laevis* egg extract spindles. *J. Cell Biol.* **182,** 715–726 (2008).
33. Helenius, J., Brouhard, G., Kalaidzidis, Y., Diez, S. & Howard, J. The depolymerizing kinesin MCAK uses lattice diffusion to rapidly target microtubule ends. *Nature* **441,** 115–119 (2006).

## METHODS

**Microtubules.** Microtubules were grown for 30 min at 37 °C from a 6.25 µl BRB80 solution (80 mM Pipes/KOH pH6.9, 1 mM $MgCl_2$, 1 mM EGTA) supplemented by 40 µM bovine tubulin (transport-microtubules: 25% rhodamine-labelled, 75% unlabelled; template-microtubules: 6.4% unlabelled biotinylated, 4.2% rhodamine-labelled and 89.4% unlabelled, Cytoskeleton), 1 mM Mg–GTP (Roche), 4 mM $MgCl_2$ and 5% DMSO. The mix was then resolved in 200 µl BRB80T (BRB80 containing 10 µM Taxol (Sigma)). Assembled microtubules were centrifuged in a Beckman airfuge at 100,000*g* for 5 min. The pellet was resuspended in 200 µl BRB80T. Polarity-marked microtubules were grown as described previously[33] using Alexa488-labelled tubulin for the seeds and bright rhodamine-labelled tubulin for elongation.

***In vitro* single molecule and sliding motility assays.** Microscope chambers were constructed of silanized coverslips using parafilm as spacer, such that channels of 0.1-mm thickness, 3-mm width and 18-mm length were formed. Silanization was performed as described previously[34]. To immobilize microtubules on the glass surface, channels were washed with a series of buffers. First a biotin antibody (Sigma) 1% in PBS was incubated for 5–10 min followed by 15 min incubation of 1% Pluronic F127 (Sigma) in PBS. Finally, biotinylated microtubules in BRB80T were allowed to bind to the surface for 15 min. Channels were rinsed once with BRB80T before the motility solutions were added. Motility solutions consisted of 20 mM Hepes/KOH pH 7.2, 1 mM $MgCl_2$, 0.1 mM EDTA, 0.1 mM EGTA and 5% sucrose freshly supplemented by 75 mM KCl, 0.1% Tween20, 1 mM ATP, 0.5 mg $ml^{-1}$ casein and anti-fade (40 mM glucose, 40 µg $ml^{-1}$ glucose oxidase, 16 µg $ml^{-1}$ catalase, 1 mM DTT). Motors at concentrations below 0.5 nM for single-molecule motor experiments or above 5 nM for microtubule–microtubule sliding experiments (all in motility solution) were injected to the channel and allowed to bind to the template microtubules. To verify that Ncd molecules were present as dimeric motor constructs under our buffer conditions, we performed fluorescence bleaching and gel filtration experiments (Supplementary Information, Fig. S1). For the sliding experiments, channels were washed with 60 µl motility solution after two minutes to remove unbound motors. Finally non-biotinylated transport microtubules in motility solution were added. The polarity of the template microtubules was determined using truncated GFP-labelled rat kinesin-1 (kinesin–GFP) that was purified according to published protocols[35]. Kinesin–GFP in BRB80 supplemented by anti-fade and ATP (1 mM) was added after recording sliding microtubule motility in the same field of view.

**Imaging.** Microtubules and GFP–Ncd molecules were visualized using an inverted fluorescence microscope (Zeiss Axiovert 200M, Carl Zeiss) with a Zeiss ×100 oil immersion 1.46 NA TIRF objective in combination with an Andor Ixon DV 897 (Andor Technology) EMCCD camera controlled by Metamorph (Molecular Devices Corporation). A Lumen 200 metal arc lamp (Prior Scientific Instruments) for excitation in epi-fluorescence mode and an argon-krypton mixed gas laser at 488 nm (Innova 70 Spectrum, Coherent) for TIRF-illumination were used. For dual-colour experiments, images were acquired either sequentially by switching between GFP and TRITC filters (Chroma Technology) or by dual-colour separation using a spectral beam splitter (W-view A8509, Hamamatsu) equipped with GFP and RFP filters (Chroma Technology). In the latter, the signals of the two colour channels were simultaneously recorded on two different halves of the same CCD camera chip. To align the dual-colour images with respect to each other, multi-fluorescent tetraspeck beads (0.2 µm diameter, Mo Bi Tec), diluted 200-fold in PBS, were imaged before the Ncd experiments. Image acquisition rates ranged from up to 10 frames per second in continuous acquisition mode (in the single molecule experiments) to 0.3 frames per second for sequential dual-colour imaging (in the sliding experiments). For image analysis, kymographs were generated and used for velocity analysis using Metamorph. Trajectories of parallel sliding transport-microtubules were obtained by a custom-made software based on MatLab (Mathworks).

**Protein expression and purification.** The following recombinant expression constructs were used: 1) pHis–NcF expressing unlabelled, N-terminal His-tagged full-length Ncd from pBS-ncd[9,10] and pET28a (Novagen) 2) pHis–GFP–NcF expressing GFP–Ncd, fusion of His-tag from pET30a (Novagen) up to *Nco*I site, EGFP from pEGFP–C1 (Clontech) and full-length Ncd from pBS-ncd; 2) pHis–GFP–$Ncd^{195}$ expressing GFP–$Ncd^{195}$, GFP–Ncd with deletion of Ncd amino acids 1–195; 3) pNcS–GFP–His expressing $Ncd^{349}$–GFP, fusion of Ncd fragment 1–349 with EGFP from pEGFP–C1 (Clonetech) and $His_6$-tag. pHis–GFP–NcF and pNcS–GFP–His were constructed in pET28a and pET30a vectors, respectively (Novagen). A detailed description of DNA manipulations used in the recombinant plasmids construction is provided in the Supplementary Information. The expression of Ncd proteins was carried out in *Escherichia coli* BL21 (DE3) strain (Novagen). The bacteria were induced with 0.5 mM isopropyl β-D-thiogalactopyranoside for 4 h at 25 °C, collected by centrifugation and resuspended in buffer A (20 mM Hepes/Na, pH 7.2, 1 mM $MgCl_2$, 20 mM 2-mercaptoethanol, 5 µM ADP, 0.1% Tween 20) + 300 mM NaCl and 20 mM imidazole. The culture was centrifuged again and frozen at –80°C. Frozen bacterial cells were thawed, resuspended in buffer A with 300 mM NaCl and 20 mM imidazole and disrupted using French Press (Thermo Spectronic) at 1380 bar in the presence of protease inhibitors. Clarified lysate was loaded on a Talon cobalt-affinity resin (Clontech) equilibrated with lysis buffer. After washing the column, the concentration of NaCl was linearly reduced to 100 mM using buffer A containing100 mM NaCl and 20 mM imidazole. Protein was eluted in buffer A containing 100 mM NaCl and 300 mM imidazole. Next, the peak fractions were purified on an FPLC Superdex 200 10/300 GL column equilibrated with the cobalt elution buffer. The eluted protein was supplemented with 10% w/v of sucrose, frozen in liquid nitrogen and stored at –80°C.

34. Hyman, A. A. Preparation of marked microtubules for the assay of the polarity of microtubule-based motors by fluorescence. *J. Cell Sci. Suppl.* **14,** 125–127 (1991).
35. Rogers, K. R. *et al.* KIF1D is a fast non-processive kinesin that demonstrates novel K-loop-dependent mechanochemistry. *EMBO J.* **20,** 5101–5113 (2001).

nature cell biology



DOI: 10.1038/ncb1877

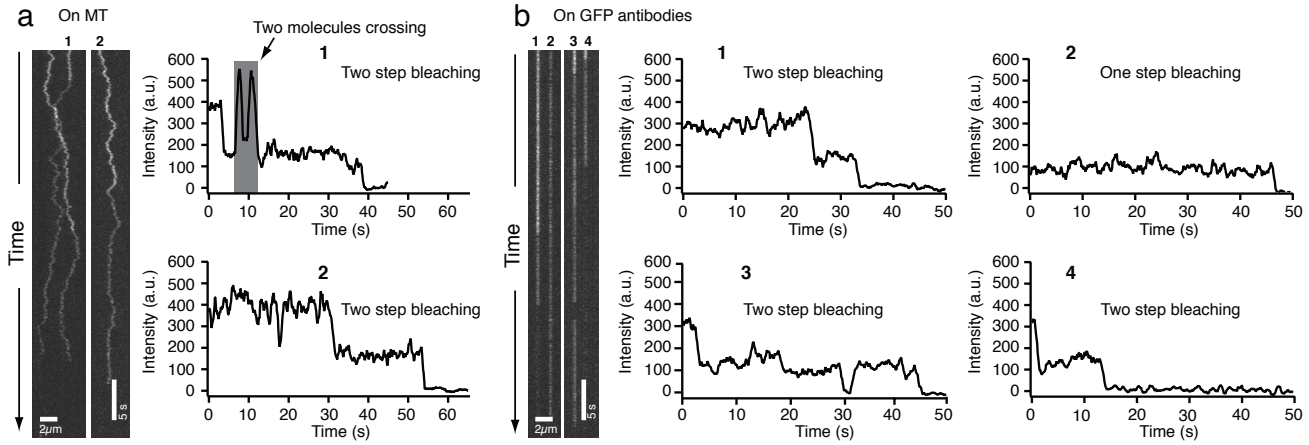


**Figure S1** Oligomeric state of Ncd motors as determined from single molecule fluorescence bleaching experiments. **a** Typical kymographs and tracked intensities of GFPNcd diffusing on template MTs in motility buffer (1 mM ATP). Bleaching in two distinct steps - indicative of GFPNcd dimers - was clearly observed in most of the cases. While the noise on the curves was mainly due to GFP-blinking, additional intensity fluctuations arose from the crossings (i.e. transient spatial overlaps) of Ncd molecules (see for example the left kymograph and trace 1, which correspond to the data of Fig. 1d in the main text). **b** Kymographs and tracked intensities of GFPNcd fixed to the surface via GFP antibodies in motility buffer (1 mM ATP). From a total of 789 randomly picked molecules, 43% exhibited two-step bleaching indicative of GFPNcd dimers. In 38% of the events, the molecules bleached in one step probably due to the previous inactivation or non-functionality of one of the GFPs. Moreover, part of these events might have originated from the rapid (and with our time resolution non-resolvable) bleaching of two GFPs after each other. In 5% of the events, bleaching appeared to occur in more than two steps. This behaviour is not speaking against the hypothesis of GFPNcd being dimeric molecules, because the spatially coinciding binding of more than one GFPNcd molecule to the same surface spot (via the same or close-by antibodies) can not be ruled out. In 14% of the events, no clear bleaching steps were detectable. In summary, the presented GFPNcd bleaching experiments verify that Ncd molecules were present as dimeric motor constructs under our buffer conditions.

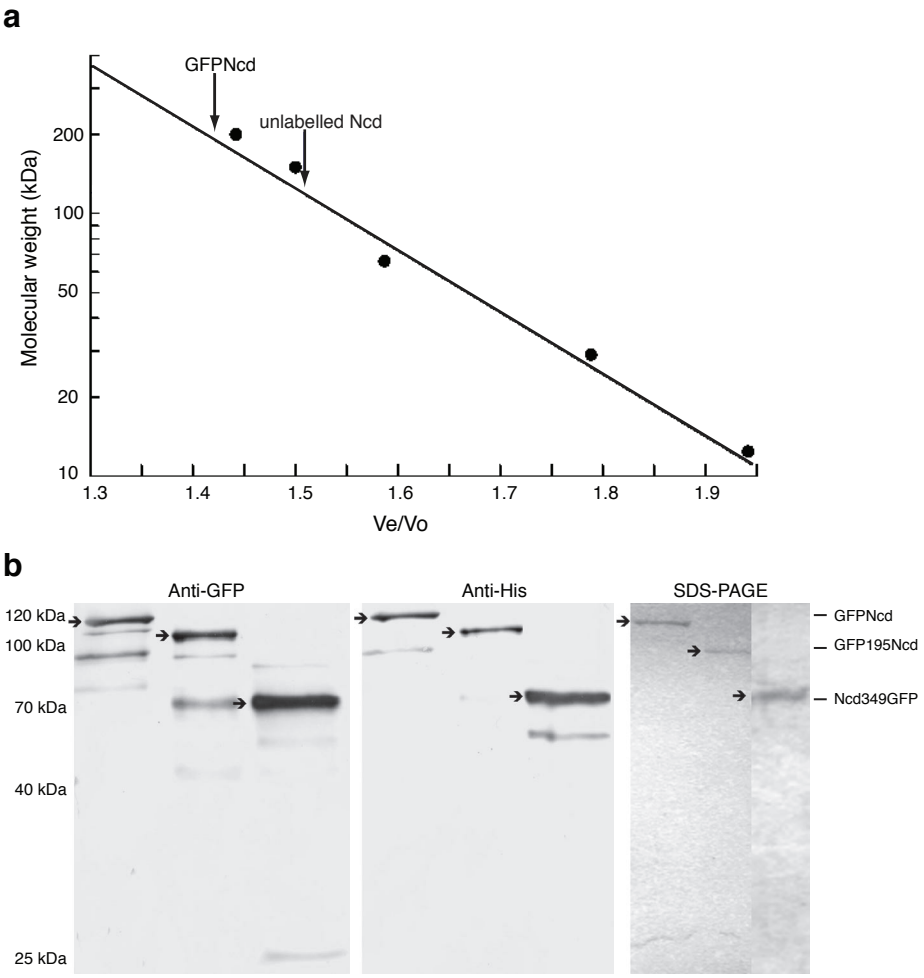


**Figure S2** Gel filtration and SDS PAGE of Ncd proteins. **a** Size exclusion chromatography: The calibration graph (points and linear fit) shows the ratio of elution volume to void volume for the used standard proteins (Supplementary Information Methods section) plotted against their logarithmic molecular weight. The arrows show the obtained ratios for GFPNcd and unlabelled full length Ncd. Each investigated protein did elute within a single peak indicating that the used protein was not composed of several populations of monomers, dimers and multimers. Relating the elution volume to the void volume yielded an approximate molecular weight of 195 kDa for the full length GFPNcd (expected molecular weight of 224 kDa for dimers and 112 kDa for monomers). Unlabelled full length Ncd yielded a molecular weight of about 120 kDa (expected molecular weight of 158 kDa for dimers and 79 kDa for monomers). All obtained molecular weights were about 30 kDa lower than the expected molecular weights. This, most likely, resulted from the fact that Ncd exhibits a more elongated structure rather than being completely globular. Nevertheless, the obtained data does indicate that the used proteins had neither formed multimers nor existed as monomers. **b** Western blots using anti-GFP polyclonal antibody (*left*), monoclonal anti-His antibody (*middle*) and Coomassie stained gel (*right*). Numbers on the left correspond to the molecular weights of some of the standards used. Arrows indicate purified proteins corresponding to GFPNcd, GFP195Ncd and Ncd349GFP (from left to right).

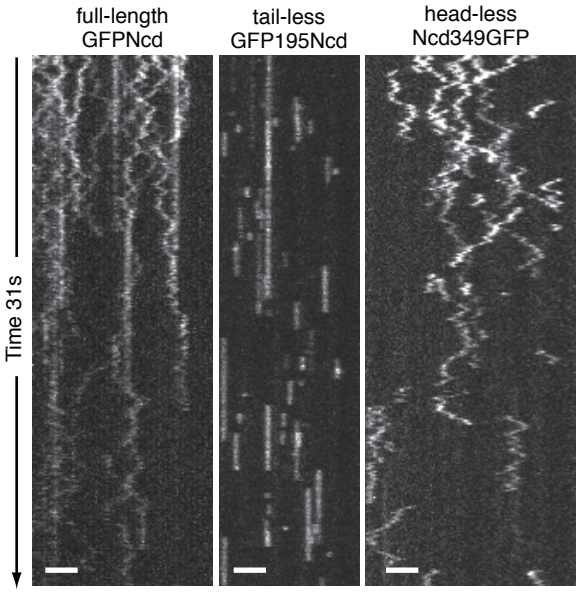


**Figure S3** Ncd interaction with MTs in AMPPNP. Typical kymographs of different, single molecule GFP-labelled Ncd constructs imaged by TIRF microscopy in the presence of 1 mM AMPPNP show that: (i) GFPNcd diffuses but also exhibits long periods of static binding, (ii) GFP195Ncd exclusively shows static binding, and (iii) Ncd349GFP diffuses in a very similar manner to the ATP condition. Occasional events of short-termed stationary binding were most likely related to degraded motors with impaired ATP hydrolysis. Scale bars: 3 μm.

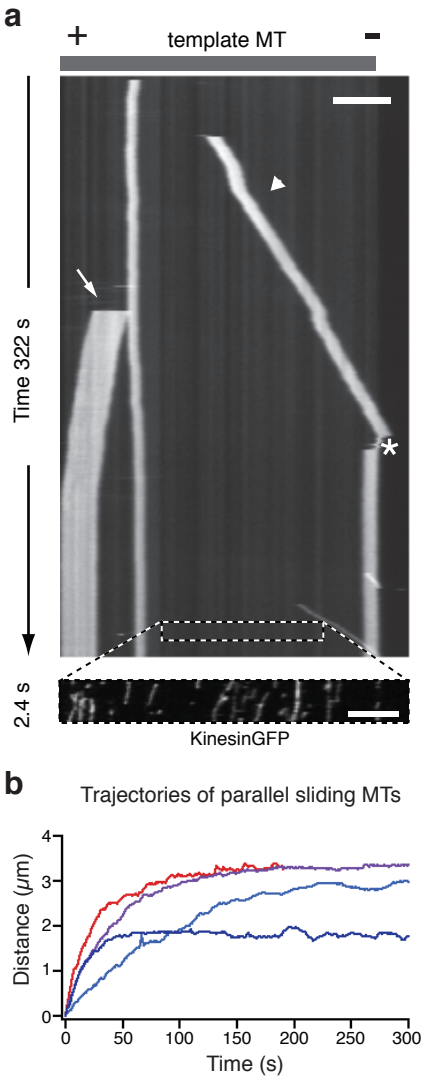


**Figure S4** Slow-down of transport MTs during parallel sliding events. **a** Typical kymograph illustrating the dynamic interactions of several transport MTs with a template MT (schematically depicted above the kymograph, scale bar: 5 μm). Robust sliding of transport MTs exclusively occurred towards the minus end of the template MT (arrowhead). After reaching the MT end, the transport MT swivelled for a short time, reoriented and got stuck (asterisk). Transport MTs that moved in opposite direction, towards the plus-ends of the template MT, showed only short motility before they statically crosslinked (arrow). The thin trajectories on the lower right correspond to additional, robustly sliding transport MTs of short lengths (Supplementary Information Movie M7). The polarity of the template MT was determined by the kymograph of GFP-labelled kinesin-1 molecules, moving towards the MT plus ends (dotted box in the lower panel, scale bar: 2 μm). **b** Quantitative analysis of MT translocation during four parallel sliding events showed a gradual decrease of the sliding velocity over time (*Time* = 0 indicates the landing of the transport MTs). After about 100s of interaction most of the transport MTs had stopped to move

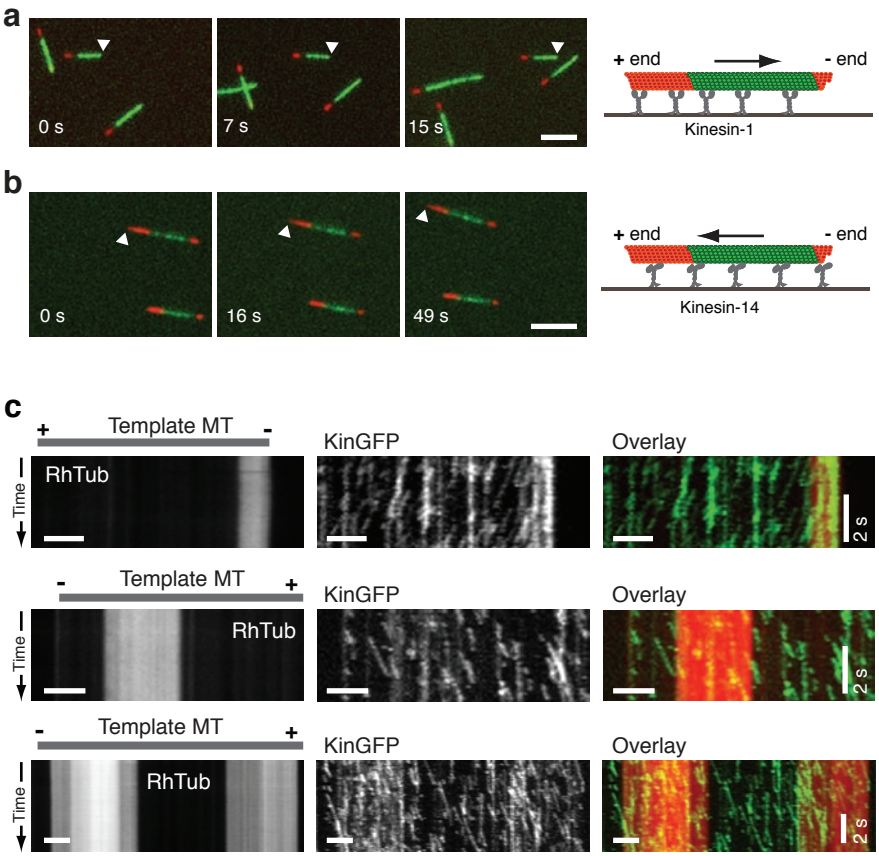


**Figure S5** Polarities of transport- and template MTs. **a** We verified the goodness of the polarity-marked MTs by gliding assays on kinesin-1 surfaces. Polarity-marked MTs were gliding with the short red extensions (i.e. their minus ends) leading (arrowheads). Note, that - because the fluorescence images in the red and the green channel were acquired with a short temporal delay - the green seed overlaps with the short red extension on the leading MT minus end. From a total of 221 observed MTs, 194 MTs (88%) clearly showed a short red extension on one side of the green seed and a longer red extension on the other side. All of these MTs were gliding with the short extension (i.e. their minus ends) leading. Scale bar: 5 µm. **b** Gliding motility experiments on Ncd-coated (kinesin-14) surfaces: MTs were gliding with their plus ends leading (arrowheads). 92% of 130 observed MTs clearly showed a short red extension on one side of the green seed and a longer red extension on the other side. 94% of these MTs were gliding with the long extensions (i.e. their plus ends) leading. The small number of MTs (6%) apparently moving into the other direction was most likely caused by MT breakage, after which the originally long red extension finally became the shorter one. Similarly, when performing Ncd MT-MT sliding experiments with polarity-marked transport MTs on Ncd-decorated template MTs (see Fig. 2a-c and Movie M4), 81% of 26 observed transport MTs clearly showed a short red extension on one side of the green seed and a longer red extension on the other side. 95% of these MTs were sliding with the long extensions (i.e. their plus ends) leading. It was therefore not necessary to perform all experiments with polarity-marked MTs, as the leading ends of the transport MTs sliding on Ncd-decorated template MTs (similar to gliding on an Ncd-coated surface) reliably marked the MT plus ends. Scale bar: 5 µm. **c** Kinesin-1 directions (KinGFP) together with the final parts of the MT kymographs from the main text: top panel corresponds to Fig. 3a, middle panel corresponds to Fig. 4a, bottom panel corresponds to Fig. 4b. Horizontal scale bars: 3 µm.

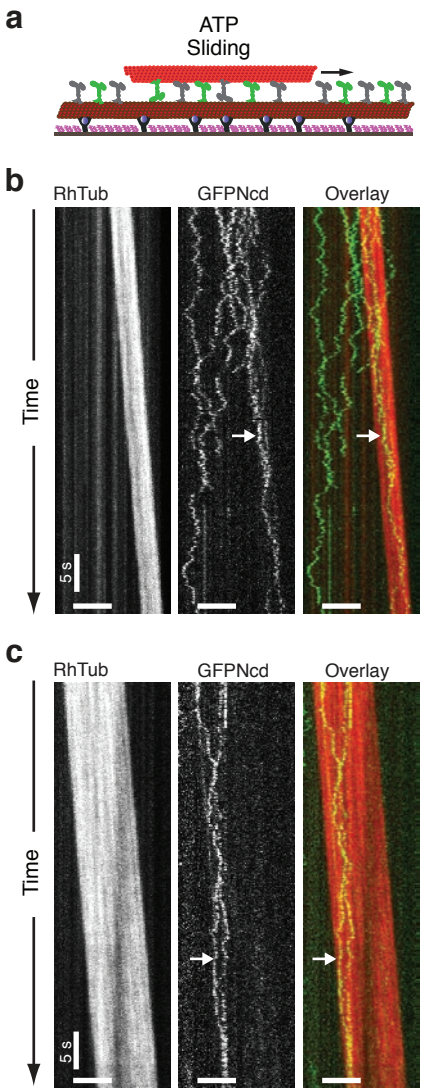


**Figure S6** Diffusion of individual GFPNcd motors in the overlap region between sliding MTs. **a** Schematic diagram of the spiking assay. Template MTs (dim red) were preincubated with a mixture of GFPNcd and unlabelled Ncd. Then, non-decorated transport MTs (bright red) were added. **b and c** Typical dual-colour kymographs of sliding transport MTs with the corresponding GFPNcd signal. Both, inside and outside the MT overlap regions we found GFP-Ncd molecules to diffuse and we never observed any directed motion or static fixation in the overlap region. Interestingly, a number of GFPNcd molecules appeared to be either cotransported with the sliding transport MT (arrow in b) or mainly interacting with the template MT (arrow in c). Horizontal scale bars: 5 µm.

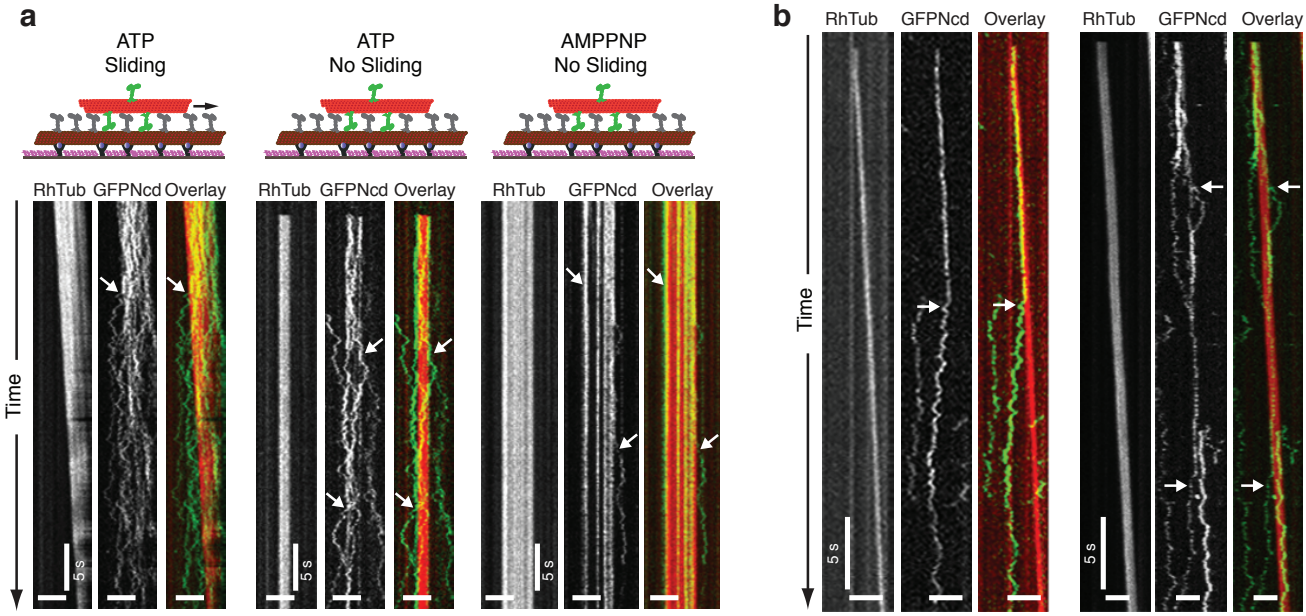


**Figure S7** Transfer of individual GFPNcd molecules between transport and template MTs in the presence of ATP and AMPPNP. In order to analyse if single motors have the capability to switch between interacting MTs, brightly-labelled rhodamine transport MTs were decorated with GFPNcd. The template MTs (dim red) were preincubated with unlabelled Ncd in order to increase the landing rates of transport MTs. Using dual colour TIRF microscopy we were able to follow single motors switching between MTs. **a** Typical dual-colour kymographs of Ncd mediated MT-MT interactions in ATP and AMPPNP. **Left panel:** In the presence of ATP, similar to the spiking experiments described in Fig. S6, GFPNcd molecules diffused in the overlap region between sliding MTs. With progressing time, GFPNcd transfered to the template MT and diffused away from the overlap region (arrow). **Middle panel:** In the presence of ATP, GFPNcd molecules diffused in the overlap region between statically crosslinked MTs. Similar to the results in the left panel, GFPNcd molecules were capable of transfer to the template MT and diffusion away from the overlap region (arrow). This indicates that MT sliding is not required for motor switching. **Right panel:** In order to elucidate if ATP hydrolysis was necessary for motor transfer we preformed the same experiments in the presence of 1 mM AMPPNP. Here, MT sliding was never observed. Moreover, Ncd was mainly linked stationary to the MTs in the overlap region and the capability to diffuse on either MT was greatly reduced most likely due to the static binding of the motor domains (heads). Horizontal scale bars: 5 µm. **b** Additional dual-colour kymographs of sliding transport MTs and interacting single GFPNcd molecules in the presence of ATP. Single GFPNcd molecules were clearly able to interact via their tails with the transport MTs as indicated by the cotransportation. However, these molecules often switched their interaction from the transport to the template MT, frequently diffusing away from the overlap region (arrows). Interestingly, after transfer to and diffusion on the template MT, a number of motors were observed to repeatedly return into the overlap region. Horizontal scale bars: 3 µm

**Supplementary Movie Legends**

**Movie S1** GFPNcd single molecules (green) interacting with MTs (red) (scale bar: 3 µm, total time 25 s, real time playback).

**Movie S2** GFP195Ncd single molecules (green) interacting with MTs (red) (scale bar: 3 µm, total time 25 s, real time playback).

**Movie S3** 349NcdGFP single molecules (green) interacting with MTs (red) (scale bar: 3 µm, total time 25 s, real time playback).

**Movie S4** Sliding of polarity-marked transport MTs (green seeds and red extension, where the longer extensions mark the MT plus ends) on template MTs (dimly labelled in red) (scale bar: 5 µm, total time 588s, 75x sped-up playback).

**Movie S5** GFPNcd (middle panel and green signal in lower panel) switches between transport (bright) template (dim) MTs (upper panel and red signal in lower panel). (scale bar: 3 µm, total time 138s, 10x sped-up playback).

**Movie S6** GFPNcd (green) accumulates at the minus ends of parallel, statically crosslinked MTs (red). Moreover, the movie shows another example of anti-parallel sliding and parallel static crosslinking.(scale bar: 5 µm, total time 508s, 35x sped-up playback).

**Movie S7** Sliding of transport MTs (bright) on template MTs (dim) (scale bar: 5 µm, total time 347s, 10x sped-up playback).

## Supplementary Methods

**DNA manipulations:** Recombinant plasmid for expression of the full length Ncd in E. coli was constructed by amplification of the full length Ncd coding sequence from plasmid pBS-ncd with primers Ncdf: ATGCATATGGAATCC CGGCTACC and Ncdr: AGCTCGAGTTAT TTATCGAAACTGCCGCTGT adding NdeI and XhoI sites respectively (underlined). PCR product cut with NdeI and XhoI was ligated into pET28a vector (Novagen) digested with the same enzymes producing plasmid pHisNcF expressing full length Ncd protein with N-terminal His-tag. N-terminal fusion of GFP with Ncd was constructed by replacement of NcoI-NdeI fragment of pHisNcF with NcoI-BfaI fragment from pEGFP-C1 plasmid (Clontech) resulting in plasmid pGFPNcF expressing Ncd with N-terminal EGFP fusion but without His-tag. To add N-terminal His-tag preceding the EGFP sequence KspI-NcoI fragment of pGFPNcF was replaced with KspI-NcoI fragment from pET30a vector (Novagen). This construct (pHisGFPNcF) expresses the fusion protein containing His-tag, GFP and Ncd (GFPNcd). The plasmid pHisGFP195Ncd expressing GFP195Ncd (N-terminal fusion of His-tag and EGFP to Ncd fragment 196-700) was constructed by "inside-out" PCR of pHisGFPNcF with primers NcF195f: TGTTCAAGGCCCGCTTC and NcF195r: TATGAGATCCGGTGGATCCC. The reaction product was phosphorylated with T4 Polynucleotide kinase and circularized by ligation. The first step of Ncd349GFP construction was cloning the EGFP coding sequence as a NcoI-SalI fragment from pEGFP-C1 into the pET30a vector resulting in plasmid pET30EGFP. Then the Ncd coding sequence (aa 1-349) was amplified from pHisGFPNcF with primers NcFSzfNde: TATCATATGGAATCCC GGCTACCGAAACC and NcFSzrNco: ATCCATGGCGATGTTGCCGCGCAGGTCC adding NdeI and NcoI sites respectively (underlined). PCR product cut with NdeI and NcoI was ligated into pET30EGFP digested with the same enzymes producing plasmid pNcSGFPHis. Correctness of all DNA manipulations described above was confirmed by DNA sequencing.

**Size exclusion chromatography*:*** The dimeric structure of the Ncd proteins was confirmed by size exclusion chromatography. Protein samples were run in motility buffer on Superdex 200 PC 3.2/30 columns on an AKTA Purifier system (GE Healthcare). The column was calibrated with a gel filtration molecular weight marker set (Sigma) containing cytochrome c from horse heart (12.4 kDa), carbonic anhydrase from bovine erythrocytes (29 kDa), bovine serum albumin (66 kDa), alcohol dehydrogenase from yeast (150 kDa), β-amylase from sweet potato (200 kDa) and Blue Dextran (2000 kDa, used to measuring column void volume). The apparent molecular weights of the analysed Ncd samples were calculated by comparing their $V_e/V_0$ values to the calibration curve.

**Gliding motility assays:** Flowcells were prepared as described in the main text, however using non-silanized glass. Surfaces were blocked by 5 min incubation with casein (0.5 mg/ml). After 5 min either a kinesin-1 (in 1 mM ATP [Roche], 0.2 mg/ml casein in BRB80) or Ncd (in motility buffer used for the sliding assay, main text) was flown in. Another 5 min later polarity-marked MTs were applied in motility buffer.

**GFPNcd photobleaching:** Flowcells were prepared as described in the main text. Single GFPNcd molecules were immobilized to the surface using anti-GFP antibodies. Imaging was performed in motility buffer. Taking intensities from GFPNcd signals and subtracting the background using Metamorph revealed the photobleaching behaviour. Obtained intensities were smoothened by a moving average (box width of 9 points) and plotted using Igor (WaveMetrics, Lake Oswego, Oregon 97035 USA).